Cite this article
Aguirre Castillo J, Broström M and Eriksson M (2023)
Phase evolution and burnability of cement raw meal.
Advances in Cement Research **35(12)**: 577–587,
https://doi.org/10.1680/jadcr.23.00034

Research Article
Paper 2300034
Received 01/03/2023;
Accepted 17/05/2023;
First published online 14/06/2023

Advances in Cement Research

Phase evolution and burnability of cement raw meal

José Aguirre Castillo
Doctoral student, Centre for Sustainable Cement and Quicklime Production, Department of Applied Physics and Electronics, Umeå University, Umeå, Sweden; Thermochemical Energy Conversion Laboratory, Department of Applied Physics and Electronics, Umeå University, Umeå, Sweden; Heidelberg Materials Cement Sverige AB, Slite, Sweden (Orcid:0000-0002-4219-1226) (corresponding author: jose.aguirre@umu.se)

Markus Broström
Professor, Centre for Sustainable Cement and Quicklime Production, Department of Applied Physics and Electronics, Umeå University, Umeå, Sweden; Thermochemical Energy Conversion Laboratory, Department of Applied Physics and Electronics, Umeå University, Umeå, Sweden (Orcid:0000-0003-1095-9154)

Matias Eriksson
Adjunct Associate Professor, Centre for Sustainable Cement and Quicklime Production, Department of Applied Physics and Electronics, Umeå University, Umeå, Sweden; Thermochemical Energy Conversion Laboratory, Department of Applied Physics and Electronics, Umeå University, Umeå, Sweden; Swedish Mineral Processing Research Association (MinFo), Stockholm, Sweden (Orcid:0000-0002-8230-8847)

The use of high-temperature X-ray diffraction (HT-XRD) to study the mass transfer of raw meal constituents towards forming clinker phases and the occurrence of free lime (calcium oxide), also known as burnability, was assessed. A measuring strategy with temperature ranging from 1000°C to 1450°C was developed and compared with a conventional burnability method. The free lime determined by the methods showed that HT-XRD produced good results for the evaluation of burnability. In addition, HT-XRD revealed the formation of intermediate phases, providing insight into early reactions in a cement kiln. The particle size of quartz was found to affect crystal expansion of the phase at a high temperature, subsequently affecting the formation of silica polymorphs. The different raw meals used in this study also indicate that the formation of different silica polymorphs affects the formation of C_2S. The lack of knowledge regarding the influence of β-quartz on the reduction of free lime is highlighted.

Keywords: characterisation techniques/clinkering/clinkering reactions/phase transition

Introduction

Cement is the traditional binder in concrete, which is used in almost all construction, from small structures to large infrastructures. However, cement production accounts for 8% of global carbon dioxide emissions, consequently contributing to climate change (Andrew, 2019). About half of the carbon dioxide emitted during cement production is generated from the combustion of fossil fuels to achieve material temperatures of 1450°C. The other half is released when heating the raw meal, which is mainly limestone. Calcium carbonate ($CaCO_3$) is the primary carbonate in limestone, and carbon dioxide emission occurs according to Reaction I.

I. $CaCO_3\ (s) \rightarrow CaO\ (s) + CO_2\ (g)$

A reduction in carbon dioxide emissions from combustion can be achieved by replacing fossil fuels with alternative fuels, optimising the burners and calciners in the system, introducing new forms of heating or capturing the carbon dioxide from the process (Hills *et al.*, 2016; Hökfors *et al.*, 2014, 2015; Worrell *et al.*, 2013). Furthermore, cement manufacturers are aiming to replace pure limestone with secondary stone and calcium-carrying waste materials from other industries, such as metallurgical slags (Del Strother, 2019; Viggh *et al.*, 2021). Replacing the raw materials affects the heat needed for the formation of clinker phases. Using an alternative raw material may be beneficial for net carbon dioxide reduction but can increase the heat consumption of the process. However, alternative raw materials may contain fluxing elements, such as fluorine, thus reducing the energy consumption (Taylor, 1997).

In ordinary Portland cement (OPC), free lime (calcium oxide (CaO)) reacts with silica, alumina and ferric oxide in the raw meal and forms clinker phases. C_3S ($3CaO.SiO_2$) is the main clinker phase that contributes most to compressive strength development; it is formed according to Reaction II. Reaction III shows the formation of C_2S ($2CaO.SiO_2$), which also contributes to the compressive strength development of cement, but to a lesser extent. Reactions IV and V show the formation of C_3A ($3CaO.Al_2O_3$) and C_4AF ($4CaO.Al_2O_3.Fe_2O_3$). C_3A has a minor impact on compressive strength development and affects the setting of cement paste. The effect of C_4AF on the development of compressive strength is negligible (Beaudoin and Odler, 2019).

II. $CaO + 2CaO.SiO_2 \rightarrow 3CaO.SiO_2$

III. $2CaO + SiO_2 \rightarrow 2CaO.SiO_2$

IV. $3CaO + Al_2O_3 \rightarrow 3CaO.Al_2O_3$

V. $4CaO + Al_2O_3 + Fe_2O_3 \rightarrow 4CaO.Al_2O_3.Fe_2O_3$

The lime saturation factor (LSF), silica ratio (SR) and alumina modulus (AM) are calculated from the contents of oxides (wt%) in the raw meal and clinker, and these parameters are used in quality control of the chemistry of the raw materials to obtained the desired/optimal phase composition in the clinker. The LSF (expressed as %), SR and AM are calculated as:

1. $$LSF = \frac{100 \times CaO}{(2.8 \times SiO_2) + (1.18 \times Al_2O_3) + (0.65 \times Fe_2O_3)}$$

2. $$SR = \frac{SiO_2}{Al_2O_3 + Fe_2O_3}$$

3. $$AM = \frac{Al_2O_3}{Fe_2O_3}$$

The LSF, typically 96% of oxides in the clinker, describes the expected ratio of C_3S to C_2S in the clinker and the residual free lime. The SR, typically 2.5, is regularly used to control the expected ratio of silicates (C_3S and C_2S) to aluminates (C_3A and C_4AF) of the clinker. The AM is guidance for the C_3A to C_4AF ratio and is usually around 1.6 (Harrisson, 2019).

The LSF is used as a guide for controlling residual free lime in clinker. At LSF > 100%, equilibrium moves towards the free-lime-rich region and hence calcium oxide can form in the clinker. However, in clinker production, free lime is produced at LSF less than 100%. The formation and reduction of free lime are affected by the properties of the raw meal (e.g. homogeneity, particle size distribution, mineralogy) and process parameters such as the residence time at high temperature and the maximum burning temperature (Fundal, 1979).

Since intermediate phases and the incremental evolution of clinker phases in rotary kilns of cement plants cannot be studied in real time, the properties of the raw meal have to be studied in detail. The term 'burnability' of raw meal, commonly used in industry, has been given different definitions. For example, Taylor defines burnability as 'the ease with which free lime can be reduced to an acceptable value in the kiln' (Taylor, 1997: 72). Lea defines it as 'the ease with which alite forms in the hottest part of the kiln' (Del Strother, 2019: 31). Chatterjee states 'the burnability of a cement raw mix conceptually denotes the amount of mass transfer of its constituents with ease or difficulty to the clinker phases' (Chatterjee, 1983: 71). Conventional laboratory methods determine burnability by measuring residual free lime at different time and temperature schemes. A raw meal with alleged good burnability is expected to form the desired clinker phases and low residual free lime. If, for example, one or many raw meal properties impede the formation of clinker phases and cause a high content of free lime, the burnability is considered poor. Even though the rate of combination of the calcium oxide component in clinker phases involves great complexity, the burnability methods used today do not measure phases other than free lime.

A review of the literature on conventional methods for burnability testing revealed they can be divided into experimental and theoretical methods. These methods are listed in Tables A1 and A2 of the Online Supplementary Appendix.

The experimental methods involve the production of granules or pellets of raw meal, which are heated to one or more temperatures relevant to the formation and reduction of free lime. After heating, the concentration of free lime is determined and, in some cases, normalised for interpretation. Process parameters such as the atmosphere inside the kiln, residence time in the burning zone and burning temperature are disregarded. Therefore, the results from laboratory tests mainly reflect the impact of the raw meal properties on the reduction of free lime with increasing temperature (Chatterjee, 1983).

The theoretical methods require chemical analysis of the raw meal in order to calculate the LSF and SR. In cement production, the higher the SR, the more silicates are formed, and more heat is required for more silicates to form (Taylor, 1997). A higher SR also leads to less alumina and iron oxide, which have fluxing properties for forming clinker phases. Thus, a higher SR is interpreted as being detrimental to burnability. A higher LSF negatively affects the burnability of the raw meal because the formation of C_3S requires higher temperatures. The theoretical burnability methods also consider the mineralogy of the raw meal and particle size effects. For this, sieve analysis is used and is performed by regular sieving. The sieve residue can then be analysed for the mineral's calcite, quartz and acid-insoluble components. Coarse calcite and quartz are traditionally estimated from chemical analysis or by optical microscopy of the sieve residue.

In addition to conventional burnability methods (see Tables A1 and A2 in the Online Supplementary Appendix), some authors have studied the phase evolution of raw meals with additional techniques such as X-ray diffraction (XRD) and clinker microscopy (Punmatharith, 2010; Theisen, 1992). In early studies, the peak intensities in XRD scans of different samples were compared. More recent studies have quantified the phase composition using the Rietveld method (Bouregaya, 2018). The development of XRD instruments, software and quality reference data has resulted in popularity of the Rietveld method for quality control in cement plants (Goswami and Panda, 1999; Uhlig *et al.*, 2008).

There are some other drawbacks to the conventional methods besides those already mentioned. The experimental burnability methods have some safety issues as they involve working with materials at high temperatures, as shown in the Online Supplementary Appendix (Table A1). Furthermore, the uncertainty in the theoretical methods increases with the uncertainty of each analysis needed (chemical analysis, sieving and mineral characterisation).

In situ powder diffraction has been used to characterise C_2S clinker phases at high temperatures (De La Torre *et al*., 2007), while in situ high-temperature XRD (HT-XRD) has been used to observe the phase evolution of clinker phases (Shirahama *et al*., 2015), the effects of foreign ions in the formation of clinker phases (Marchi *et al*., 2007; Segata *et al*., 2019) and the formation of the ternesite phase (Ullrich *et al*., 2021). A limitation of HT-XRD is that there is limited structural data for clinker phases at high temperatures, making their refinement and quantification difficult. Remy *et al*. (1997) conducted an HT-XRD study in which structural changes of the C_2S phases were followed; they showed that it is possible to modify ambient structural data to fit high-temperature phases.

The objective of the work described in this paper was to study the phase evolution of six industrial raw meals using a newly developed HT-XRD method. Ambient structural data were modified to fit high-temperature phases to facilitate their quantification by the Rietveld method and further interpretation of the results. The HT-XRD results accounted for a large number of phases formed during heating, including free lime. The results were compared with free lime measured using a conventional burnability method.

Materials

Six industrial raw meals used to produce OPC were studied. The properties of the raw meals, production process information and the type of corrective materials used to adjust each raw meal's chemistry are provided in Table 1.

- Samples A1 and A2 were from the same plant, milled in a vertical mill 2 years apart. Both samples comprised a small portion of blast-furnace slag.
- Samples B1 and B2 were from the same plant, milled in a ball mill 2 years apart. They differed in the balance of high-grade limestone used. B2 consisted of less high-grade limestone and more impure low-grade limestone and, consequently, fewer corrective materials such as raw sand were used.
- Sample C was milled in a vertical mill. This sample contained the smallest number of corrective materials as the limestone from this plant can be very impure.
- Sample D was ground in an aero fall mill and contained metallurgical slag.

Methods

Chemical analysis with X-ray fluorescence (XRF) and carbon–sulfur analyser

The chemical compositions of the six samples were determined using an accredited XRF calibration with fused beads in a Panalytical Axios XRF instrument (Malvern Panalytical, UK). The beads were made by propane heating with di-lithium tetraborate 98.0% flux medium at 1100°C in a Fluxana Vulcan fusion machine (Fluxana, Germany). The XRF analyses were complemented with carbon and sulfur data obtained using a Leco CS230 carbon–sulfur analyser (Leco, USA) and loss on ignition (LOI) measured at 950°C in a muffle furnace.

Particle size distribution and manual sieve analysis

Particle size distributions were studied using a Malvern Mastersizer 2000 (Malvern Panalytical, UK) with water dispersion. To determine the coarse fractions of calcite (> 125 μm) and quartz (> 45 μm) in the samples, each raw meal was air sieved with mesh sizes of 45, 90, 125 and 200 μm.

Conventional burnability tests

Seven dry pellets of each raw meal were produced in moulds of 25 mm diameter using a pressure of 6 t. The compression resulted in a pellet thickness of about 15 mm. All pellets of the same material were loaded into platinum crucibles, placed in a laboratory furnace and then heated at a rate of 10°C/min. Sampling started at 1000°C, followed by temperatures of 1100, 1200, 1300, 1350, 1400 and 1450°C. Each temperature was held for 20 min before each sample was air-cooled, ground and analysed for free lime using the wet chemical method (Schläpfer–

Table 1. Raw meals and process information

	A1, A2	B1, B2	C	D
Raw materials	■ High-grade limestone ■ Low-grade limestone ■ Ground slag, Blast-furnace slag and iron corrective ■ Alumina corrective	■ High-grade limestone ■ Low-grade limestone ■ Sand (two types)	■ High-grade limestone ■ Low-grade limestone ■ Silica sand	■ High-grade limestone ■ Low-grade limestone ■ Sand ■ Metallurgical slag ■ Alumina corrective
Type of mill	Vertical mill	Ball mill	Vertical mill	Aero fall mill
Type of kiln system	Pre-heater calciner	Pre-heater	Pre-heater calciner	Pre-heater calciner
Type of clinker cooler	Crate cooler	Satellite cooler	Crate cooler	Crate cooler

Bukowski method (Bukowski, 1933)) and XRD. This method involves diluting a sample in ethylene glycol, titrating with hydrochloric acid and calculating the free lime from the molar ratio of reactants.

XRD, HT-XRD and the Rietveld method

The mineralogy of untreated samples, air-sieved samples and heated samples was analysed using XRD combined with the Rietveld method. The measurements were performed using a Panalytical X'Pert instrument (Malvern Panalytical, UK) with Bragg–Brentano geometry and Cu-Kα radiation ($\lambda = 0.15408$ nm) at 45 kV and 40 mA. The angular range $2\theta = 10$–$65°$ was investigated with a step size of 0.02° and 200 s/step using a Pixcel 1D detector. The X'pert instrument was quipped with an Anton Paar HTK 2000N high-temperature chamber (Anton Paar GmbH, Austria) for the HT-XRD measurements. The samples were placed on the heating strip in the chamber following the manufacturer's instructions. The manufacturer recommends a particle size of less than 30 μm. However, this would have caused significant alterations to the properties of the samples. Instead, all the samples were slightly milled in a Retsch MM 400 ball mill in 25 ml zirconia jars with 20 mm dia. balls. Six grams of each sample was ground at 30 Hz for 1 min. The fineness of the samples was checked by laser diffraction. The 90 μm sieve residues before and after milling are listed in Table 2. The milled samples were applied to the heating strip, achieving an area of 10×10 mm and a thickness of <0.5 mm. The temperature in the chamber was increased at a rate of 10°C/min. XRD measurements were performed at 1000, 1100, 1200, 1300, 1350, 1400 and 1450°C. The temperature was controlled by a factory-welded Pt–10% RhPt thermocouple welded to the bottom of the platinum strip right underneath the sample. Each temperature was held for 5 min before the measurement and the heating rate between each measurement was 10°C/min. The samples were then cooled at a rate of 400°C/min to 1000°C and 200°C/min to 25°C. A measurement was collected after the cooling step. The measurement window was set at $2\theta = 10$–$65°$ with a step size of 0.02° and 50 s/step. The measurements were conducted in air: no protecting gas or purge was used.

HighScore Plus 5.0 (Malvern Panalytical, UK) and structure files from the Inorganic Crystal Structure Database (ICSD) were used for mineral characterisation and Rietveld quantification of the cooled pellet samples. The high-temperature samples were also characterised using HighScore Plus, but Diffac.Topas 6.0 (Bruker AXS GmbH, Germany) and ICSD structure files were used for quantification. Structure files from the Crystallography Open Database (COD) were used when needed. A list of the structure files used is provided in Table A3 of the Online Supplementary Appendix.

Results and discussion

Results of analyses on raw mixes

The results of chemical analyses, particle size distribution, sieving and determination of coarse calcite and quartz are

Table 2. General results and main oxides measured using XRF

	A1	A2	B1	B2	C	D
Calcium oxide (CaO): wt%	42.9	42.5	42.6	42.8	43.1	43.4
Silicon dioxide (SiO_2): wt%	13.1	13.5	13.2	13.3	13.7	13.9
Aluminium oxide (Al_2O_3): wt%	3.36	3.16	3.74	3.8	3.41	3.55
Ferric oxide (Fe_2O_3): wt%	1.89	1.9	1.88	1.96	1.67	2.1
Magnesium oxide (MgO): wt%	2.85	2.95	0.907	0.874	1.37	1.92
Potassium oxide (K_2O): wt%	0.82	0.821	0.944	0.975	0.593	0.879
Sodium oxide (Na_2O): wt%	0.22	0.15	0.12	0.09	0.44	0.28
Chromium(III) oxide (Cr_2O_3): wt %	0.001	0.002	0.002	0.001	0.003	0.003
Manganese(III) oxide (Mn_2O_3): wt%	0.067	0.057	0.349	0.36	0.027	0.046
Titanium dioxide (TiO_2): wt%	0.274	0.238	0.182	0.186	0.262	0.183
Phosphorus pentoxide (P_2O_5): wt%	0.034	0.026	0.087	0.086	0.050	0.048
Vanadium pentoxide (V_2O_5): wt%	0.013	0.009	0.007	0.005	0.006	0.007
Zinc oxide (ZnO): wt%	0.057	0.053	0.003	0.002	0.001	0.014
LOI at 950°C: wt%	33.3	33.7	34.9	34.8	34.4	32.6
Carbon dioxide (CO_2): wt%[a]	34.6	34.8	35.7	35.5	37	34.2
Sulfur trioxide (SO_3): wt%[a]	1.07	1.06	0.23	0.27	0.85	0.98
Calculated LSF	102.5	99.4	100.0	99.5	99.2	97.6
Calculated SR	2.50	2.67	2.35	2.31	2.70	2.46
Calculated AM	1.78	1.66	1.99	1.94	2.04	1.69
Coarse calcite >125 μm[b]	6.0	5.5	5.0	4.4	1.7	2.4
Coarse quartz >45 μm[b]	1.4	1.0	2.8	3.0	3.9	2.2
90 μm passing (before milling)[c]	78.3	80.7	74.2	78.4	76.6	83.7
90 μm passing (after milling)[c]	95.0	89.3	91.8	91.2	85.6	94.8

[a]Measured with a carbon–sulfur analyser
[b]Analysed using an air sieve and XRD
[c]Calculated with laser diffraction

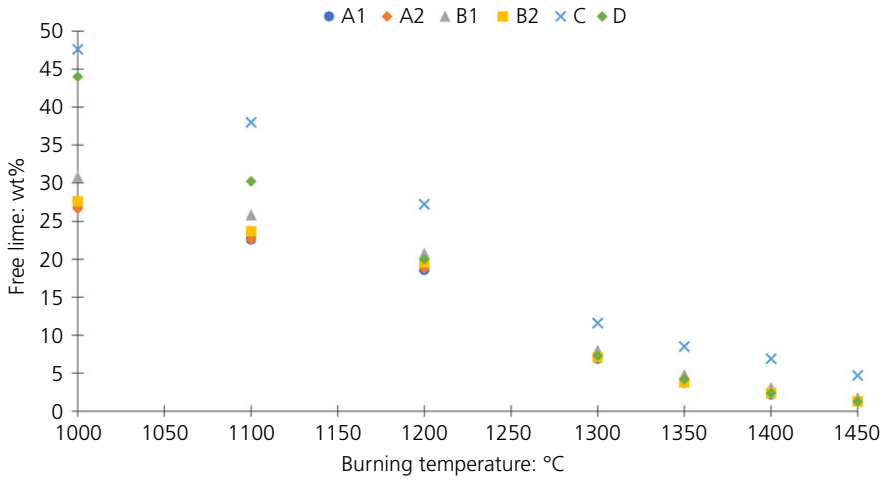

Figure 1. Free lime measurement using wet chemical method (a conventional burnability method)

presented in Table 2. The LSF, SR and AM were calculated for all samples. As mentioned earlier in the paper, the typical LSF target is 96. All the samples showed a higher LSF because they are expected to absorb fuel ashes in the kiln and the LSF target also varies from plant to plant. The amount and chemistry of ash must be included in the raw meal to clinker calculation (Aguirre Castillo and Eriksson, 2022). The SR is, however, not as dependent on fuel ashes as the LSF. As noted earlier, the SR controls the ratio of silicates to aluminates. A higher SR requires higher temperatures and a longer burning time. The AM also varied between the samples. Sieve analysis showed that sample C had the greatest amount of coarse quartz (> 45 μm), while sample A1 has the highest content of coarse calcite (> 125 μm). These two factors are expected to influence the formation of C_2S and C_3S clusters in the clinker, respectively (Fundal, 1979). The mineral composition of the initial samples is shown in the Online Supplementary Appendix (Table A4).

Results from the conventional burnability method

The free lime values measured using the conventional method (pellets) described in the section 'Conventional burnability tests' are presented in Figure 1 and Table 3. (Full results from all quantifications can be found in Tables A5 to A10 of the Online Supplementary Appendix.) All the samples heated to a temperature starting at 1000°C were fully calcined. Samples A1 and A2 showed the fastest free lime reduction, followed by samples B1 and B2, D and C. The phase compositions of all the cooled pellet samples were quantified using the Rietveld method. Figure 2 shows plots of the phase evolution of samples A1 and C. At 1000°C, sample A1 consisted of 47 wt% C_2S, mostly the β polymorph. Sample C was found to have 5.4 wt% β-C_2S and almost double the unreacted free lime, which is due to the effect of coarse quartz in the raw meal.

Table 3. Free lime measurements using the wet chemical method

	Free lime: wt%					
Temperature: °C	A1	A2	B1	B2	C	D
1000	27.0	26.6	30.8	27.6	47.6	44.0
1100	22.6	22.6	25.8	23.7	38.0	30.2
1200	18.6	18.8	20.8	19.6	27.2	20.0
1300	6.9	7.2	8.0	7.1	11.6	7.3
1350	3.7	4.0	4.8	3.8	8.5	4.2
1400	2.2	2.4	3.1	2.4	6.9	2.4
1450	1.3	1.5	1.8	1.3	4.7	1.3

It was expected from the sieve analysis that sample C would have some difficulties in the reduction of free lime and quartz. Table 2 shows that sample C had the highest content of coarse quartz (> 45 μm), followed by samples B2, B1, D, A1, and A2. However, samples B1 and B2 performed almost as well as sample A1 and showed a similar final free lime content in the 1450°C samples. Sample B2 showed smaller free lime values at lower temperatures than the longer stored sample from the same source (B1). Samples B1 and B2 also showed the highest amounts of α'H C_2S, even with the same cooling rate as the other samples. The stabilisation of α'H C_2S during cooling is known to be enhanced by higher cooling rates and stabilisers (such as phosphorus pentoxide (Taylor, 1997)), which was somewhat higher in samples B1 and B2 (Table 2). However, the difference in phosphorus pentoxide contents in samples B1 (0.087 wt%) and B2 (0.086 wt%) was not high enough compared with the other samples to draw any conclusions.

Sample D showed a slow free lime reaction at lower temperatures (1000–1200°C) and ended with a low free lime content in the 1450°C sample. This effect may be explained by the formation of stable intermediate phases at high temperatures that form from silica (SiO_2), hindering the further reaction of free

lime. The intermediate gehlenite ($Ca_2Al(AlSiO_7)$) was found in amounts of 4–5 wt% in the samples at 1000–1200°C.

Results from the HT-XRD method

As in the experimental burnability method, samples A1 and A2 showed the fastest free lime reduction and sample C was the slowest. The phase evolution plots for samples A1 and C from the HT-XRD method are presented in Figure 3. Further visual representations of the phase development of cooled pellets and high-temperature measurements of sample A1 are shown in Figures 4 and 5, respectively, with the peaks of the main phases marked on the figures. The peaks in Figure 5 shifted to the left, indicating thermal expansion of the phases. Unlike the cooled pellet samples (Figure 4), more polymorphs of the main phases were present in the high-temperature measurements (Figure 5), for example, C_2S polymorphs α, α′H and α′L. The cooled pellet samples contained mainly the β-C_2S polymorph. Quantification results for the high-temperature samples can be found in the

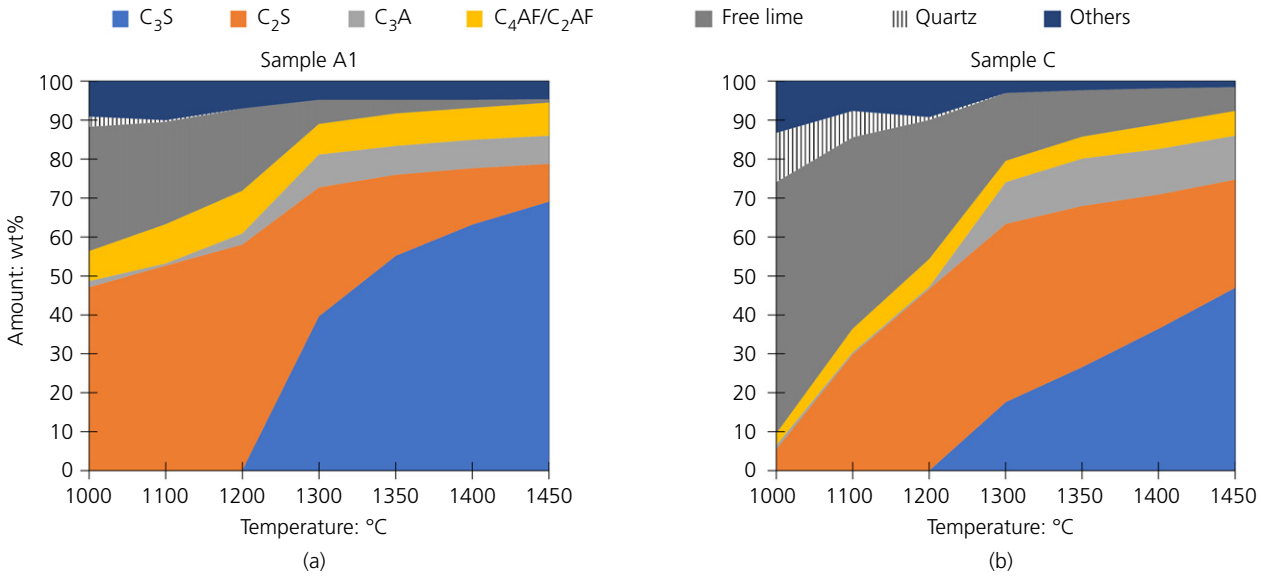

Figure 2. Phase evolution of samples A1 and C from the conventional burnability method. Each of the main clinker phases, C_3S, C_2S, C_3A, and C_4AF/C_2AF, displayed is the sum of several polymorphs. Phases designated as others are shown in the Online Supplementary Appendix (Tables A5–A10)

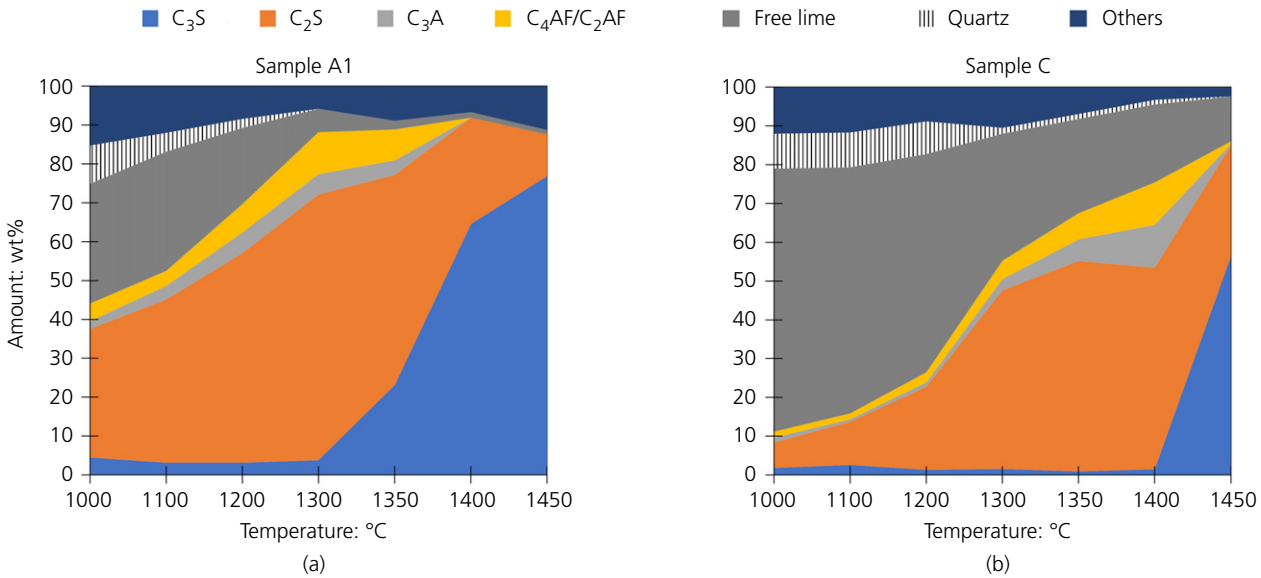

Figure 3. HT-XRD phase evolution of samples A1 and C. Each of the main clinker phases, C_3S, C_2S, C_3A, C_4AF/C_2AF, and quartz, displayed is the sum of several polymorphs. Phases designated as others are shown in the Online Supplementary Appendix (Tables A11–A16)

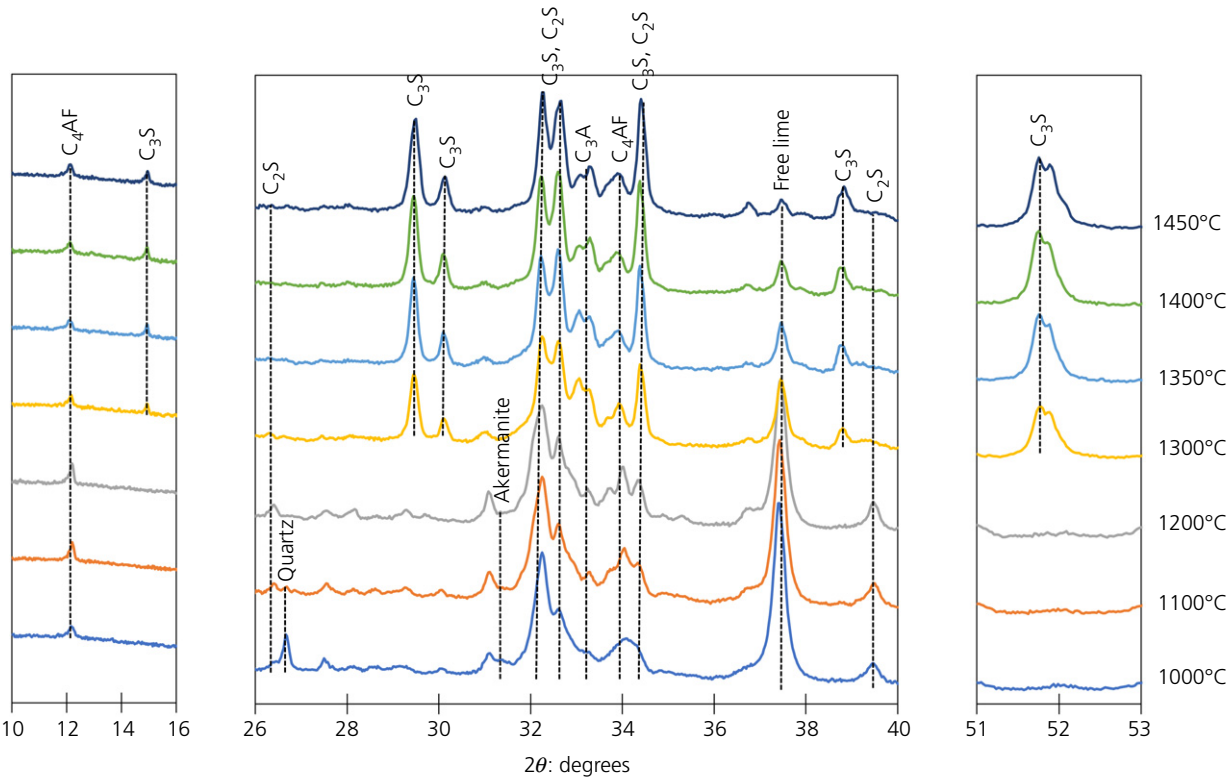

Figure 4. XRD scans of cooled pellets of sample A1 in angular ranges $2\theta = 10–16°$, $2\theta = 26–40°$ and $2\theta = 51–53°$ (Cu-Kα radiation, $\lambda = 0.15408$ nm)

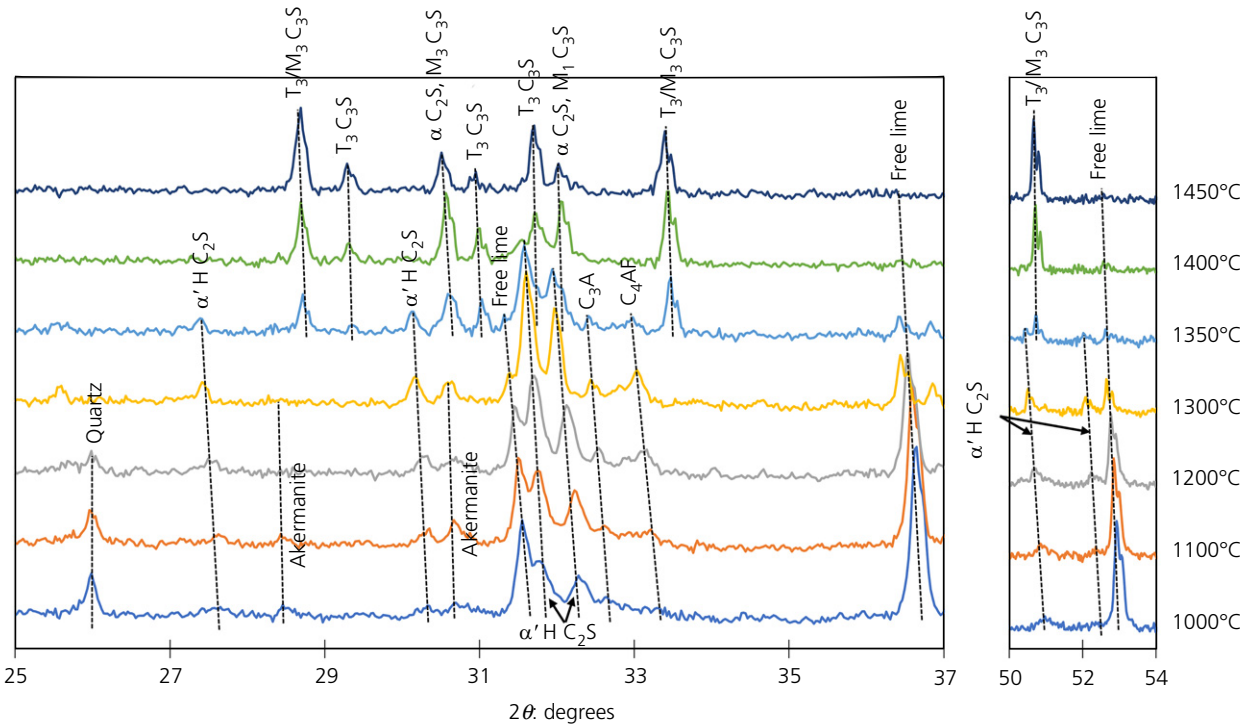

Figure 5. HT-XRD scans of sample A1 in angular ranges $2\theta = 25–37°$ and $2\theta = 50–54°$ (Cu-Kα radiation, $\lambda = 0.15408$ nm)

Online Supplementary Appendix (Tables A11–A16). Almost only C_4AF (ICSD 9197 (Colville and Geller, 1971)) could be fitted for the ferrite phase in high-temperature conditions, while C_4AF (ICSD 9197), $Ca_2Fe_{0.654}Al_{1.346}O_5$ (ICSD 98839 (Redhammer *et al.*, 2004)) and $Ca_2Fe_{1.635}Al_{0.365}O_5$ (ICSD 98826 (Redhammer *et al.*, 2004)) were used for the cooled pellet samples in the conventional method, showing the effect of cooling on the yielding of ferrite solid solution.

Almost all the high-temperature samples also showed peaks of aluminium (fitted with COD 9012955 (Owen and Yates, 1933)) and α-iron (fitted with COD 9008536 (Wyckoff, 1963)) at temperatures higher than 1400°C. The formation of pure aluminium and iron was not expected. The formation mechanism of these in the cement process has not been reported elsewhere and may be due to the conditions of the experiments. The equipment used in this study was used before in research for a master's thesis: alumina and iron were formed in the same industrial raw meal (A1) but not in a synthetic raw meal (Vikström, 2021).

Quantification of the high-temperature measurements showed results relatable to the samples burned and cooled with the conventional method. Figure 6 shows comparisons of the free lime contents obtained using the different quantification methods (wet chemical analysis and XRD–Rietveld quantification) on cooled pellets. The agreement was good for all samples. Samples C and B2, which had the two highest contents of coarse quartz. Samples C and B2, which had the two highest contents of coarse quartz, showed rather logarithmic than linear agreement towards the wet chemical analysis. The logarithmic behaviour is believed to be caused by the coarse particle size of quartz, meaning poor contact with other species in the thin sample (<0.5 mm) and resulting in weaker diffusion between particles. However, sample B2 had a relatively low free lime (2.8 wt%) at the highest temperature compared with sample C (11.3 wt%). Sample C had a higher SR, indicating lower fluxing aluminium oxide and ferric oxide, resulting in higher energy needed to reduce free lime, which, combined with coarse silica, badly affected the burnability.

Samples from the high-temperature chamber were cooled and measured after being exposed to 1450°C. The results for the cooled high-temperature samples corresponded to those of the conventional method (cooled at 1450°C) but were much higher in free lime, as seen in Figure 7, which may be an effect of poor mass transport through the thin sample. Similar correlations were found for all other phases. Measurements of more samples from different plants, in combination with clinker microscopy results, are needed to establish reliable limits for the interpretations of burnability, as done by Fundal (1979).

The cooled high-temperature samples showed amounts of periclase (magnesium oxide (MgO)) in samples A1 (5.2 wt%) and

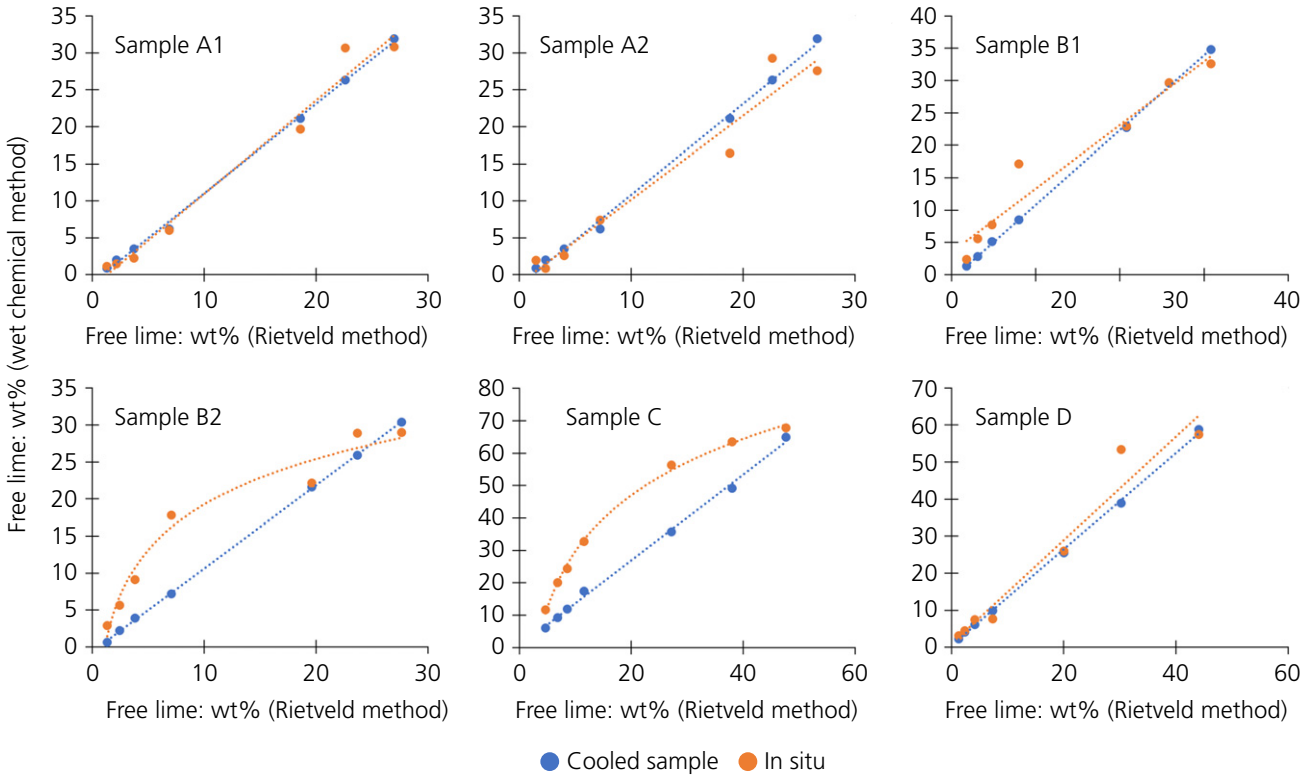

Figure 6. Comparison of free lime values obtained with the wet chemical method and the Rietveld method

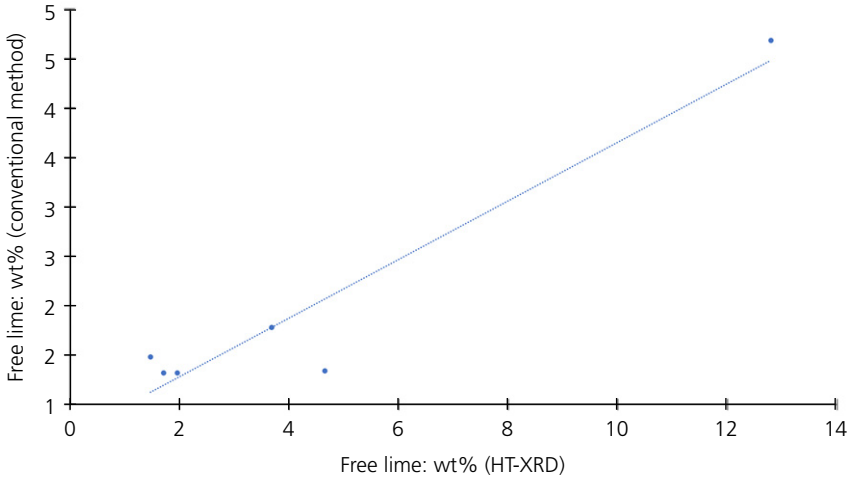

Figure 7. Comparison of final free lime values obtained using the conventional method and HT-XRD

A2 (5.1 wt%) that were somewhat high since the magnesium oxide in the raw meals was determined to be 2.85 wt% (4.27 wt% LOI-corrected) for A1 and 2.95 wt% (4.45 wt% LOI-corrected) for A2 ((Table 2)). (The results of all cooled high-temperature samples are shown in Table A17 of the Online Supplementary Appendix.) Repeated analysis of sample A1 showed similar results. The preferred orientation was used for periclase, but the main periclase peak (200; $2\theta = 42.9°$) seemed to be affected by an unknown phenomenon. The amount of periclase may also be affected by the presence of amorphous species. The use of an internal standard for identifying amorphous species was discussed when designing the experiment. However, the authors could not find a suitable standard material that would not interact with the samples or the platinum plate through all the temperatures. In addition, adding a standard after a measurement would be impossible since the sample could not be fully retrieved from the platinum plate. Otherwise, periclase was barely visible in the measurements at high temperatures. Magnesium oxide is mainly found in the stable akermanite phase ($Ca_2Mg(Si_2O_7)$) at temperatures up to 1350°C, later moving to C_3S, C_2S and C_4AF phases (Taylor, 1997).

High-temperature measurements on sample C showed a split quartz peak at around $2\theta = 26°$ at 1000°C, as shown in Figure 8. Two α-quartz structure files were refined to fit the split peak, showing unit cell volumes of 117.5 $Å^3$ (right peak) and 120 $Å^3$ (left peak) (1 $Å^3 = 0.001$ nm^3). The quartz in the raw meal had a volume of 113 $Å^3$. Quartz at 1000°C expands but does not fully transition to a high-temperature polymorph. β-quartz was identified in the measurement. The transition of α-quartz to β-quartz should occur at 573°C and the transition to *β*-tridymite at 870°C (Herfort and Macphee, 2019). Instead, intermediate silicates were detected, such as enstatite ($MgSiO_3$), melilite ($(Ca, Na)_2 (Al, Mg, Fe^{2+}) ((Al, Si) SiO_7)$) and gehlenite, which were not present in the initial raw meal. α-quartz was first depleted after

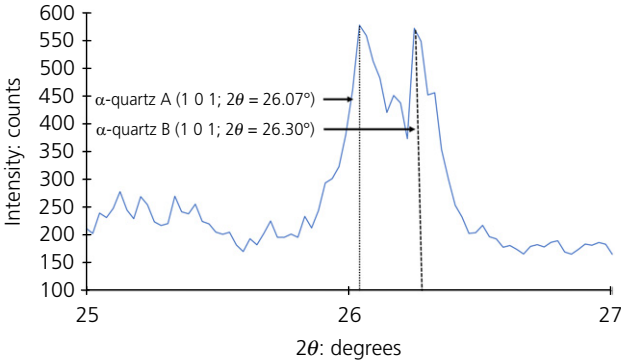

Figure 8. HT-XRD measurement on sample C at 1000°C showing a split *α*-quartz peak

1300°C in all the raw meals in this study. β-quartz was present in sample C up to 1400°C. From the amounts of coarse quartz determined by sieve analysis of samples B1 and B2, it was expected that they would have a slow free lime reduction. However, B1 and B2 performed well in both the conventional and HT-XRD methods. They differed in the amounts of gehlenite and akermanite, which persisted up to 1350°C in sample B1 and 1200°C in B2, indicating an improvement. Sample B1 and B2 formed fractions of β-quartz similar to those of samples A1, A2 and D, but not sample C. This indicates that the formation of β-quartz at high temperatures might influence the reaction with free lime and the formation of clinker phases. The quartz polymorphs of all the samples are listed in Table 4. Burte and Nicholson (1972) concluded that C_2S is the only reaction product from the reaction of β-quartz and calcium oxide in different directions of the β-quartz crystal. They referred to the study of Jander and Hoffmann (1934), in which quartz formed C_3S, C_2S, C_3S_2 and wollastonite ($CaSiO_3$), depending on the calcium oxide to silica ratio. In this study, wollastonite was only

Table 4. Quartz polymorphs determined from HT-XRD measurements

Sample		Temperature: °C					
		1000	1100	1200	1300	1350	1400
A1	α-quartz: wt%	5.0	4.4	1.7	—	—	—
	β-quartz: wt%	4.8	0.4	0.7	—	—	—
A2	α-quartz: wt%	6.2	0.9	0.6	—	—	—
	β-quartz: wt%	5.3	1.0	—	—	—	—
B1	α-quartz: wt%	2.4	1.4	0.0	—	—	—
	β-quartz: wt%	4.7	1.8	1.8	—	—	—
B2	α-quartz: wt%	3.6	1.4	1.0	—	—	—
	β-quartz: wt%	2.5	1.3	0.9	—	—	—
C	α-quartz (expanded) : wt%	1.2	0.8	0.8	—	—	—
	α-quartz-2: wt%	6.3	6.5	3.3	—	—	—
	β-quartz: wt%	1.6	1.7	4.3	1.5	1.3	1.2
D	α-quartz (expanded) : wt%	2.0	2.3	0.3	—	—	—
	α-quartz-2: wt%	4.4	—	—	—	—	—
	β-quartz: wt%	5.8	1.0	—	—	—	—

found in the cooled pellet samples using the conventional method. The periclase in the samples in this study favoured the formation of C_3MS_2 ($Ca_3Mg(SiO_4)_3$, merwinite) and C_2MS_2 ($Ca_2Mg(Si_2O_7)$, akermanite) instead of C_3S_2 ($Ca_3Si_2O_7$, rankinite). Nonetheless, the reaction mechanism of the quartz polymorphs may be studied further using HT-XRD.

Similar intermediates were found in the HT-XRD measurements, as with the samples analysed using the conventional method. Sample D contained gehlenite in the 1000°C high-temperature sample and the equivalent pellet sample. In high-temperature conditions, the gehlenite phase shifted towards the composition of akermanite at 1100°C, and the akermanite persisted up to 1400°C. Akermanite was not seen in the pellet samples of raw meal D. The transition to akermanite at high temperatures was most likely affected by poor mass transport in the thin sample compared with the pellet used in the conventional method. However, gehlenite, akermanite and melilite phases are essential for understanding the coatings formed in kilns (Taylor, 1997).

Conclusions

The evolution of phases in cement raw meals during heating was determined using HT-XRD. The free lime content measured using HT-XRD was similar to that measured using a conventional burnability method. The results showed that it is feasible to use HT-XRD as a method to determine free lime at different times and temperatures, which, at present, is usually done using conventional burnability methods. Future work might encompass the study of more raw meal samples from different plants in order to establish reliable data to facilitate the interpretation of free lime results obtained by different methods. In addition, HT-XRD can generate data for interpretation of the behaviour of raw meal in the burning process, for example, the formation of coatings by studying the evolution of gehlenite and akermanite. This study also highlights a lack of knowledge regarding the influence of β-quartz on the reduction of free lime.

Acknowledgements

The authors would like to acknowledge Rainer Backman at Umeå University for his valuable contribution, along with Heidelberg Material Cement Sverige AB and Heidelberg Materials Sement Norge AS for providing samples for this study and analytical and shared experiences. Heidelberg Material Cement Sverige AB, SMA Mineral AB, the Swedish Mineral Processing Research Association – MinFo and the Swedish Energy Agency (no. 2020-008305, Project 50893-1) are acknowledged for financial support.

REFERENCES

Aguirre Castillo J and Eriksson M (2022) Impact of solid alternative fuels on cement kiln operation. In *Proceedings of the 28th International Conference on the Impact of Fuel Quality on Power Production and the Environment, Åre, Sweden* (Markus B (ed.)). Department of Applied Physics and Electronics, Umeå University, Umeå, Sweden.

Andrew RM (2019) Global CO_2 emissions from cement production, 1928–2018. *Earth System Science Data* **11(4)**: 1675–1710.

Beaudoin J and Odler I (2019) Hydration, setting and hardening of Portland cement. In *Lea's Chemistry of Cement and Concrete*, 5th edition (Hewlett PC and Liska M (eds)). Elsevier, New York, NY, USA, pp. 157–250.

Bouregaya S (2018) *Synthèse d'un ciment alitique à moindre impact environnemental à partir de vase de barrage et utilisant le sulfate de zinc comme minéralisateur*. Doctoral thesis, L'Université De Toulouse, Toulouse, France (in French).

Bukowski R (1933) *Die Bestimmung des freien Kalkes(CaO) und des Kalziumhydroxydes($Ca(OH)_2$) in Zementklinkern, Zementen, Schlacken und abgebundenen hydraulischen Mörteln*. ETH Zürich, Zurich, Switzerland (in German).

Burte AS and Nicholson PS (1972) Influence of anisotropy and water vapor on the solid-state reaction of CaO and beta quartz. *Journal of the American Ceramic Society* **55(9)**: 469–472.

Chatterjee TK (1983) Burnability and clinkerization of cement raw mixes. In *Advances in Cement Technology* (Ghosh SN (ed.)). Pergamon, Turkey, pp. 69–113.

Colville AA and Geller S (1971) The crystal structure of brownmillerite, Ca2FeAlO5. *Acta Crystallographica Section B* **27(12)**: 2311–2315.

De La Torre AG, Morsli K, Zahir M and Aranda MAG (2007) In situ synchrotron powder diffraction study of active belite clinkers. *Journal of Applied Crystallography* **40(6)**: 999–1007.

Del Strother P (2019) Manufacture of Portland cement. In *Lea's Chemistry of Cement and Concrete*, 5th edition (Hewlett PC and Liska M (eds)). Elsevier, New York, NY, USA, pp. 31–56.

Fundal E (1979) The burnability of cement raw mixes. *World Cement Technology* **10**: 195–204.

Goswami G and Panda JD (1999) Application of XRD in a rapid quality control system of cement. *Powder Diffraction* **14(2)**: 114–117.

Harrisson AM (2019) Constitution and specification of Portland cement. In *Lea's Chemistry of Cement and Concrete*, 5th edition (Hewlett PC and Liska M (eds)). Elsevier, New York, NY, USA, pp. 87–156.

Herfort D and Macphee DE (2019) Components in Portland cement clinker and their phase relationships. In *Lea's Chemistry of Cement and Concrete*, 5th edition (Hewlett PC and Liska M (eds)). Elsevier, New York, NY, USA, pp. 57–86.

Hills T, Leeson D, Florin N and Fennell P (2016) Carbon capture in the cement industry: technologies, progress, and retrofitting. *Environmental Science & Technology* **50(1)**: 368–377.

Hökfors B, Eriksson M and Viggh E (2014) Modelling the cement process and cement clinker quality. *Advances in Cement Research* **26(6)**: 311–318, https://doi.org/10.1680/adcr.13.00050.

Hökfors B, Viggh E and Eriksson M (2015) Simulation of oxy-fuel combustion in cement clinker manufacturing. *Advances in Cement Research* **27(1)**: 42–49, https://doi.org/10.1680/adcr.13.00068.

Jander W and Hoffmann E (1934) Reaktionen im festen zustande bei höheren temperaturen. XI. Mitteilung. die reaktion zwischen calciumoxyd und siliciumdioxyd. *Zeitschrift für Anorganische und Allgemeine Chemie* **218(2)**: 211–223 (in German).

Marchi M, Costa U and Artioli G (2007) Influence of SO_3 and MgO on clinker mineralogical composition: an 'in-situ' HTXRD study. In *Proceedings of the 12th International Congress of Cement Chemistry, Montreal, Canada* (Beaudoin JJ, JM M and Raki L (eds)). Cement Association of Canada, Ottawa, ON, Canada.

Owen EA and Yates EL (1933) Precision measurements of crystal parameters locality: synthetic sample: at T = 18 C. *Philosophical Magazine* **15(98)**: 472–488.

Punmatharith T, Rachakornkij M, Imyim A and Wecharatana M (2010) Co-processing of grinding sludge as alternative raw material in Portland cement clinker production. *Journal of Applied Sciences* **10(15)**: 1525–1535.

Redhammer GJ, Tippelt G, Roth G and Amthauer G (2004) Structural variations in the brownmillerite series Ca2(Fe2–xAlx)O5: single-crystal X-ray diffraction at 25°C and high-temperature X-ray powder diffraction (25°C≤T≤1000°C). *The American Mineralogist* **89(2–3)**: 405–420.

Remy C, Andrault D and Madon M (1997) High-temperature, high-pressure X-ray investigation of dicalcium silicate. *Journal of the American Ceramic Society* **80(4)**: 851–860.

Segata M, Marinoni N, Galimberti M *et al.* (2019) The effects of MgO, Na_2O and SO_3 on industrial clinkering process: phase composition, polymorphism, microstructure and hydration, using a multidisciplinary approach. *Materials Characterisation* **155(23)**: 109809.

Shirahama N, Harada T, Yamashita M and Tanaka H (2015) In-situ observation of the clinker formation process by a high-temperature X-ray diffraction. *Cement Science and Concrete Technology* **69(1)**: 82–87.

Taylor HFW (1997) *Cement Chemistry*. Thomas Telford Publishing, London, UK.

Theisen K (1992) The influence of raw mix burnability on cement clinker. *World Cement* **23**: 17–23.

Uhlig S, Schmidt R and Knorr K (2008) Quantification of minerals for quality and process control – made easy by XRD (X-ray diffraction) analysis. *Industrial Minerals Conference, Athens, Greece*.

Ullrich A, Garbev K and Bergfeldt B (2021) In situ X-ray diffraction at high temperatures: formation of Ca_2SiO_4 and ternesite in recycled autoclaved aerated concrete. *Minerals* **11**: 789.

Viggh E, Eriksson M, Wilhelmsson B and Backman R (2021) Early formation of belite in cement clinker raw materials with slag. *Advances in Cement Research* **33(6)**: 249–256, https://doi.org/10.1680/jadcr.19.00150.

Vikström A (2021) *Separate Calcination in Cement Clinker Production*. Master's thesis, Umeå University, Umeå, Sweden.

Worrell E, Kermeli K and Galitsky C (2013) *Energy Efficiency Improvement and Cost Saving Opportunities for Cement Making*. Energy Star, U.S. Environmental Protection Agency, Washington, DC, USA.

Wyckoff RWG (1963) Sample at T=298K Body centered cubic, bcc, structure. In *Crystal Structures*, 2nd edition. Interscience Publishers, New York, NY, USA, pp. 7–83.

How can you contribute?

To discuss this paper, please submit up to 500 words to the editor at support@emerald.com. Your contribution will be forwarded to the author(s) for a reply and, if considered appropriate by the editorial board, it will be published as a discussion in a future issue of the journal.